Experimental screening of intermetallic alloys for electrochemical CO_2 reduction

van den Berg, Daniël; Brouwer, Johannes C.; Hendrikx, Ruud W.A.; Kortlever, Ruud

DOI
10.1016/j.cattod.2024.114805

Publication date
2024

Document Version
Final published version

Published in
Catalysis Today

Catalysis Today 439 (2024) 114805

Contents lists available at ScienceDirect

Catalysis Today

journal homepage: www.elsevier.com/locate/cattod

Experimental screening of intermetallic alloys for electrochemical CO_2 reduction

Daniël van den Berg [a], Johannes C. Brouwer [b], Ruud W.A. Hendrikx [c], Ruud Kortlever [a,*]

[a] Large-Scale Energy Storage Section, Process & Energy Department, Faculty of Mechanical Engineering, Delft University of Technology, Leeghwaterstraat 39, Delft 2628 CB, the Netherlands
[b] Materials Science and Engineering, Delft University of Technology, Mekelweg 2, Delft 2628 CD, the Netherlands
[c] Surface and Interface Engineering, Materials Science and Engineering Department, Faculty of Mechanical Engineering, University of Technology, Mekelweg 2, Delft 2628 CD, the Netherlands

ARTICLE INFO

Keywords:
Electrocatalysis
Electrochemical CO_2 reduction
Intermetallic alloys
Screening
Spark Plasma Sintering

ABSTRACT

In this study, we experimentally screen a promising class of intermetallic alloys for the electrochemical reduction of CO_2 toward hydrocarbon products. Based on previous DFT-based screening papers, combinations of strongly CO-binding metals such as iron, cobalt, and nickel with weakly CO-binding metals such as gallium, aluminium or zinc were selected as potentially promising catalytic materials. Despite the challenging production of these alloys, we report a general two-step synthesis method for intermetallic alloys and discuss the specific synthesis conditions that must be taken into account when synthesising these materials. After their synthesis, we use a recently developed differential electrochemical mass spectrometry (DEMS) setup to rapidly quantify the CO_2 reduction products over a range of potentials. Almost all newly developed intermetallic catalysts are shown to produce methane and ethylene, while the CoSn catalyst showed higher selectivity towards formate production. However, all tested catalysts mostly produced hydrogen and only reduce CO_2 to a small extent, despite the favourable computational screening results. We discuss possible reasons for this discrepancy and outline a more holistic approach for linking future DFT studies with experiments.

1. Introduction

We currently find ourselves in an energy transition from a society based on fossil fuels to one based on renewable energy. This transition requires many technological changes and innovations. One of the main challenges is developing new processes to produce bulk chemicals using renewable energy and circular raw materials rather than extracting and producing them from fossil feedstocks. If successful, these processes can provide sustainable commodity chemicals in the chemical industry and transportation fuels. Additionally, these processes can serve as a storage medium for renewably generated electricity and as such level off fluctuations between renewable energy generation to match global demand. Currently, synthetic fuels can only be made at an industrial scale via an indirect route, where CO_2 and electrochemically produced hydrogen react to form (higher) hydrocarbons or alcohols. However, it would be more efficient to produce these synthetic fuels directly from CO_2 and water via an electrochemical reaction. This process can be performed at milder conditions and can potentially provide a more direct, efficient route compared to the thermochemical production route.

Unfortunately, it has proven difficult to find an electrocatalyst that selectively reduces CO_2 to a (higher) hydrocarbon or alcohol. Most transition metals generally reduce CO_2 to 2-electron reduction products such as CO and formate. Only copper is able to produce highly desired hydrocarbons and alcohols [1–4]. Copper is able to reduce CO_2 beyond CO due to its optimal binding strength of the key surface intermediate CO* [5]. This intermediate is crucial for the reduction of CO_2 towards synthetic fuels. If the binding strength is too strong, for instance with nickel, iron and palladium, the catalyst surface is poisoned by CO* and only hydrogen is produced [6]. On the other hand, if the CO* binding strength is too weak, which, for instance, is the case with gold, silver and zinc, CO* desorbs before it gets the chance to be reduced further [7]. However, the CO* binding strength is not the only parameter that enables copper to reduce CO_2 towards further reduced products. Additionally, copper has no underpotential deposited hydrogen (H_{upd}) [5], displays a favourable binding strength of C* [8] and an ideal atomic spacing that enables it to perform C-C bond forming reactions via CO

* Corresponding author.
E-mail address: R.Kortlever@tudelft.nl (R. Kortlever).

https://doi.org/10.1016/j.cattod.2024.114805
Received 14 March 2024; Received in revised form 29 April 2024; Accepted 9 May 2024
Available online 16 May 2024

dimerization [9]. The major disadvantages of copper are that it produces (oxygenated) hydrocarbons unselectively at relatively high overpotentials and experiences stability issues making it less attractive for industrial applications [3,10,11].

Alloying different metals provides an alternative approach to design new catalyst materials that could have superior catalytic performances and superior stability. By alloying, the binding strength of multiple key intermediates can be finetuned by varying the alloy ratio or their geometric structure. However, the combination of more than two metals massively expands the number of possible combinations and materials to be tested compared to the limited selection of only pure metals. Synthesizing and testing each of these materials individually would be an enormous and unpractical task. Fortunately, the activity of a material toward CO_2 reduction to further reduced products can be predicted to some extent using density functional theory (DFT) calculations, allowing the relatively fast screening of many different materials. In the literature, many studies have reported simulations on a range of different materials and predictions on potentially interesting materials [12–16]. Two of these DFT studies, Li et al. and Tran et al., concluded that the combination of strong CO-binding metals (iron, nickel, cobalt, and palladium) together with weak CO-binding p-block metals (aluminium, gallium, tin, and zinc) can provide good candidates for CO_2 reduction towards further reduced products [12,13]. Moreover, combinations of these metals can form a subclass of alloys referred to as intermetallic alloys. The two metal constituents of these materials are arranged in a well-defined crystal structure with fixed atom positions and site occupancies leading to long-range ordering [17]. This well-defined structure can give intermetallic alloys an edge over ordinary bimetallic alloys as it provides a more homogeneous catalyst surface and better control over the catalyst design. Moreover, intermetallic compounds are known for their excellent long-term stability.

However, only a few of these non-copper intermetallic compounds of this combination have been studied for their CO_2 reduction activity. So far only alloy combinations of nickel-group 13 have been tested in the literature [18–20]. This could be because of their difficult synthesis process or because of slow analysis techniques to quantify the formed products. Therefore, the goal of this study is twofold: first to design a generalized method for the synthesis of different intermetallic alloys and second to rapidly screen the activity of these alloys for their CO_2RR activity using a recently developed differential electrochemical mass spectrometry (DEMS) setup to show the effectiveness of this technique [21]. Overall, six different intermetallic alloys, namely AlFe, AlNi, CoSn, NiGa, $FeGa_3$, and $FeZn_4$, were synthesised, characterized, and tested in for their catalytic activity towards CO_2 reduction. Each of these alloys was predicted to be a selective binary alloy for the further reduction of CO_2 beyond CO by either one of the two previously mentioned DFT screening studies [12,13]. We find that although most of these alloys produce hydrocarbon products during CO_2 electroreduction, they mostly produce hydrogen and only reduce CO_2 to a limited extent. Therefore, we outline several causes for the observed mismatch between the computational and experimental results. Moreover, we advocate for a more holistic approach to computational material screening for CO_2RR to improve its accuracy.

2. Experimental

2.1. Materials

All solutions were prepared using ultrapure water (Millipore Milli-Q gradient A10 system, 18 MΩ cm) and reagents of high purity. Electrolytes were prepared using $KHCO_3$ (≥ 99.95 %, trace metal basis, Sigma-Aldrich). As counter electrode, glassy carbon counter electrodes (25×25×1 mm) were purchased from HTW (Sigradur®, polished). For the calibration of the liquid products, formic acid (≥ 95 % Sigma-Aldrich), methanol (≥ 99.9 % Sigma-Aldrich), ethanol (≥ 99.8 %, Sigma-Aldrich), 1-propanol (≥ 99.9 % Sigma-Aldrich) and allyl-alcohol (≥ 99 % Sigma-Aldrich) were used to make dilution series. The gaseous products (hydrogen, carbon monoxide, methane, and ethylene) were calibrated using calibration mixtures with concentrations between 8000 ppm and 50 ppm of analytes balanced in CO_2 (Linde). To equilibrate the incoming electrolyte into the cell with CO_2 and in the DEMS setup highly pure CO_2 gas was used (4.5 N, Linde). To synthesise the alloys, pure metals were used: Iron powder (99.9 %, 100–325 mesh, ChemPur), Nickel powder (99.99 %, 100 mesh, MaTeck), Cobalt powder (99.9 %, 200 mesh, MaTeck), Aluminium powder (99.95 %, 100–325 mesh, MaTeck), Gallium pellets (99.999 %, < 3 mm, MaTeck), Tin granules (99.9 %, ~3 mm, MaTeck), Zinc granules (99.999 %, 1–5 mm, MaTeck).

2.2. Electrochemical measurements

All electrochemical experiments were performed using a Biologic SP-200 potentiostat, using a RE-6 Ag/AgCl reference electrode (BASi). The measurements were performed in a PEEK electrochemical flow cell where the electrolyte flowed over the electrodes in ten parallel channels with 1 ml/min to improve mass transfer to the electrode surface. All electrochemical measurements were measured in triplicate. A cationic membrane (Nafion 117) was used to prevent any crossover of formed products. Further details about the electrochemical cell can be found in section S1 of the supporting information. As a counter, a polished glassy carbon (HTW, Sigradur ®) was used. Prior to every measurement run, the glassy carbon electrode was polished using a 3 μm diamond paste (DP-floc, Struers, USA) and a microfiber cloth (DP-floc, Struers, USA) to remove any contaminants. After polishing the glassy carbon electrode was washed with Milli-Q water. The PEEK cell was stored every night in an aqueous 20 vol% HNO_3 solution to prevent any build-up of contaminants. Further details about the DEMS setup used to quantify the electrochemical performance are given in section S2 of the supporting information.

2.3. Intermetallic alloy synthesis

Thermal diffusion was used in this study to obtain the desired alloys. For this method, the pure metals were mixed in their desired atomic ratios and placed inside a crucible with a lid. Typically, around 20 g of each metal was used. The crucible and contents were subsequently heated up to a temperature based on the phase diagram of the alloy in question. The $FeZn_4$ alloy suffered from the high vapour pressure of zinc. Therefore, instead of placing the metals in an open crucible, they were placed in a quartz ampule which was purged with argon and sealed off under vacuum. This ampule was placed in a tube furnace and heated up. To prevent the formation of different intermetallic phases, the ampule was first heated up to 670 °C with a heating rate of 5 °C/min to form the Γ-phase. Then, the ampule was cooled down with a cooling rate of 5 °C/min to 550 °C to obtain the desired Γ_1-phase [22]. The CoSn and NiGa samples were synthesized in a tube oven in an alumina crucible under a constant argon flow of 250 ml_n/min. Their heating rate was 5 °C/min. The other three samples were synthesized in a pressureless SPS setup and were heated and cooled at a rate of 15 °C/min. During the pressureless SPS synthesis, the die was kept at an overpressure of 20 mbar with argon.

However, after their synthesis, most alloys were often irregular in size, porous, or fragile and could therefore not be used directly in an electrochemical flow cell. Therefore, the metals were crushed into a fine powder and sintered in carbon moulds using spark plasma sintering (SPS) at a pressure of 50 MPa. Only the NiGa sample was obtained as a single piece after melting and therefore did not need a spark plasma sintering treatment. Finally, the obtained disks were sanded to remove the carbon outer layer and polished to obtain a flat surface. The precise synthesis conditions used for each alloy combination can be found in Table 1.

Table 1
Synthesis conditions of the six prepared alloys. In the second and third columns, the temperature and duration of the thermal diffusion step are shown. In the final two columns, the temperature and duration of the subsequent SPS step are shown. *The CoSn, $FeZn_4$, and NiGa samples were synthesized in a tube oven. Furthermore, the NiGa sample was obtained as one piece and therefore did not need to be spark plasma sintered.

Alloy	Thermal diffusion temperature (°C)	Thermal diffusion duration (h)	SPS temperature (°C)	SPS duration (h)
AlFe	1250	2.5	1050	2
AlNi	1250	2.5	1050	1.5
CoSn*	1200	24	900	1.5
$FeGa_3$	900	1.5	700	1.5
NiGa*	1200	24	-	-
$FeZn_4$*	670–550	12–24	500	2.5

2.4. XRD measurements

For the XRD measurements, several settings and apparatus were used. For the CoSn and NiGa a Bruker D8 Advance diffractometer Bragg-Brentano geometry and Lynxeye-XE-T position sensitive detector was used. The source was Cu Kα radiation at 45 kV and 40 mA. The variable divergence slit was set to 12 mm irradiated length, and the air scatter screen height to 5 mm. The detector settings were set to "high resolution". For the $FeGa_3$ sample a graphite monochromator and Vantec position-sensitive detector with graphite monochromator was used with Co Kα radiation at 40 kV and 40 mA. Also, the air scatter screen height was set to 8 mm. The AlNi, AlFe, and $FeZn_4$ were measured with a Bruker AXS D2 Phaser using radiation Cu Kα radiation at 30 kV and 10 mA current. For the iron samples that were measured with this setup, the lower discriminator value was set at 0.190 V and the upper value was set at 0.25 V.

2.5. Electrode preparation

After sintering, the residual carbon was removed from the metal surface using P180-grid sandpaper and sanded into the desired dimensions for the electrochemical DEMS cell [21]. Subsequently, the electrodes were sanded stepwise with sandpaper of finer grid sizes (P320, P800, P1200. P2000). Finally, the alloyed electrodes were polished using 3 μm and 1 μm diamond paste (DP-floc, Struers, USA) and a microfiber cloth (DP-floc, Struers, USA). Prior to each measurement, the polishing steps were repeated to remove any roughened surface and contaminants from the electrodes. Finally, the electrodes were washed using ultrapure water and subsequently dried using compressed nitrogen or argon before cell assembly.

2.6. Product analysis

2.6.1. Mass spectrometry settings

Mass spectrometry was performed on a Hiden HPR40 dissolved-species mass spectrometer. All incoming species were first ionized and subsequently accelerated with a voltage of 3 V and an electron current of 500 μA at an electron energy of 70 eV, except for mass 28 and mass 2. These two masses were accelerated using an electron beam with a current of 50 μA at an electron energy of 19.5 eV. Finally, all masses were detected by a Secondary Electron Multiplier (SEM) which was set at a voltage of 935 V. The calibration method for each of the major reduction products (gasses and alcohols) is discussed in more detail in section S3 of the supporting information.

2.6.2. Carboxylic acid detection and quantification

Since carboxylic acids are in the deprotonated form in the 0.1 M $KHCO_3$ electrolyte (pH = 6.8), they cannot pass the DEMS membrane and hence cannot be quantified with the mass spectrometer. Instead, carboxylic acid production was detected and quantified using high-performance liquid chromatography (HPLC). Following the obtained residence time distribution of the DEMS [21], the electrolyte exiting the liquid DEMS inlet was collected 7 minutes after the chronoamperometry measurement started. The concentration of carboxylic acids was measured by injecting 100 μl into the HPLC (Agilent Technologies 1260 Infinity, USA) to quantify the formed carboxylic acid products. For the catalysts tested in this study only formic acid was detected. The HPLC was calibrated with a dilution series in the range of 0.01 mM to 5 mM of formic acid (95 %, Sigma–Aldrich). The flowrate of the eluent (1 mM H_2SO_4 (aq)) was set to 0.6 ml min^{-1} and the measurement ran for one hour. The HPLC used two Aminex HPX-87 H columns (Biorad) in series heated to 60 °C. A refractive index detector (RID) was used for the detection of products.

3. Results & discussion

3.1. Synthesis and characterization of intermetallic alloys

The main challenge in testing different intermetallic alloys for their electrochemical CO_2 reduction activities was their synthesis. While there are several methods in the literature to produce specific intermetallic combinations, these methods are often not transferable to other combinations. Furthermore, wet synthesis methods are often unreliable since there is often not an a-priori known relationship between the starting ratio between the elements and the resulting desired composition [17]. Instead, the alloys of interest were synthesised using thermal diffusion by mixing the pure metal constituents in a crucible and heating the mixture. Here, the different metals diffuse into one another and form the desired alloy phase. Although this method is rather straightforward, several considerations had to be made. For instance, the choice of crucible material was limited due to the nature of all the metals involved; carbon or silicon carbide crucibles will leach carbon into the resulting alloy, while boron nitride will react with both cobalt and nickel at higher temperatures. Therefore, high-purity alumina crucibles were used, except in the case of cobalt-containing alloys, since cobalt oxide and alumina from the crucible react at 1200 °C to form the pigment cobalt blue [23]. Moreover, the temperature could not be increased too much as the crucibles often cracked at higher temperatures. Therefore, the higher melting metals could not be liquefied and had to dissolve into the liquid to form the desired alloy below their melting point. To enhance the mixing of the constituents and shorten the diffusion time of the metals into one another, the high-melting-point metals were added as a fine powder. Finally, due to the low boiling point and high vapour pressure of zinc, this metal was difficult to work with. To prevent the zinc from boiling off, the temperature of these alloys was kept below 900 °C and the metals were sealed in a quartz ampule under vacuum. All alloys were prone to oxidation and were therefore synthesised under an inert argon atmosphere. An oxygen filter was used to keep the oxygen level at ppb levels. However, gallium is much more prone to oxidation and even trace amounts of oxygen below 1 ppb for prolonged periods of time caused the formation of a layer of gallium oxide (Ga_2O_3). Therefore, the gallium alloys were synthesized in a pressureless SPS setup where the presence of graphite foils at high temperature removes any trace of oxygen from the atmosphere and by using a much shorter synthesis time of 1.5 hours.

Fig. 1 shows the XRD analysis to indicate the presence of the desired intermetallic compounds. In some cases, relatively small amounts of other phases are detected, which could be due to the incomplete thermal diffusion of both metals into one another. However, in all cases, the relative amount of these other compounds is negligible compared to the desired material following Rietveld refinement. In the case of AlFe, 9 % of Al_2O_3 was detected, while in the CoSn sample, 5 % Co_2Sn_3 was observed.

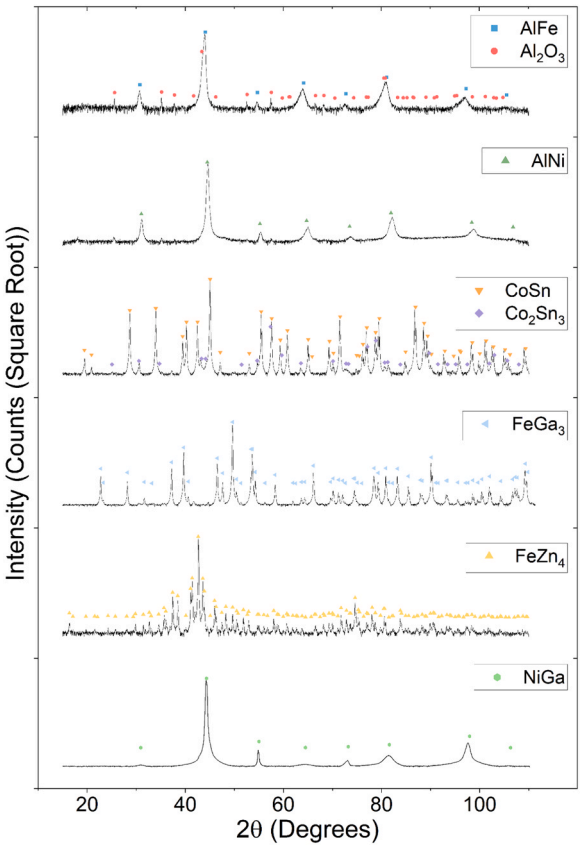

Fig. 1. XRD diffractograms of the six investigated alloys. The symbols mark the location of the standard diffraction patterns of each respective material. The square root of the intensity is taken to be able to better distinguish the smaller peaks in the diffractogram.

3.2. Electrochemical measurements

The CO_2 reduction activity of the intermetallic compounds was evaluated using a recently designed DEMS setup [21]. The mathematical model to deconvolute the mass peak signal is described in section S4 of the supporting information. Consecutive fifteen-minute chronoamperometry measurements were conducted with decreasing potential steps of 0.2 V from −0.3 V vs. RHE to −1.3 V vs. RHE, using 0.1 M $KHCO_3$ as electrolyte. The potential range is chosen based on the conditions outlined in the screening paper that formed the basis of the selection of alloys for this study [12]. All catalysts were stable when emerged in the electrolyte at open circuit potential, with the exception of $FeZn_4$. Due to the ignobility of zinc, the material corrodes and dissolves to form Zn^{2+} and hydrogen. Therefore, the catalyst activity of this catalyst was tested at a more negative potential range between −0.7 V vs. RHE and −1.5 V vs. RHE. Moreover, the potential was always kept at −0.7 V vs. RHE prior to the chronoamperometry measurements to keep corrosion to a minimum.

Fig. 2 presents the results of the chronoamperometry measurements. At lower potentials, the catalysts do not reach a hundred percent faradaic efficiency balance (see section S5 of the supporting information), most likely due to side reactions where metal oxides on the surface are reduced. These oxide layers can be formed during exposure to air prior to or during the assembly of the cell. It is also possible that at lower potentials, hydrogen is adsorbed on the surface. These reactions cannot be quantified by the DEMS and will therefore not account for the faradaic balance. Eventually, most of the surface oxides are reduced and at higher potentials, the faradaic efficiency balances are closed.

Most catalysts produce methane and ethylene with AlNi being the most active towards hydrocarbon formation, displaying an onset potential for methane production of −0.5 V vs. RHE. Ethylene formation is further observed on $FeGa_3$, $FeZn_4$, and NiGa. AlFe produces only methane and seems to be unable to form a C-C bond necessary to produce ethylene. Among all the tested catalysts only CoSn does not produce any hydrocarbons, but instead only reduces CO_2 to CO and formate. It is, however, quite active towards formate production with an onset potential of −0.3 V. Its inability to form any further reduced products is in stark contrast to the prediction from Li et al. that CoSn should be selective towards C_{2+} products [12].

Since the catalysts in this study have mostly not been tested in literature for their CO_2RR performance before, it is difficult to compare the results with literature sources. Nevertheless, their results are in reasonable accordance with other literature sources that tested comparable materials. Paris and colleagues tested Ni_3Al around −0.8 V vs. RHE and found that the catalyst produced mostly hydrogen and some carbon monoxide when a buffered solution was used of 0.1 M K_2SO_4 with $KHCO_3/CO_2$ at a pH of 6.5 [18]. Additionally, Torelli et al. found that NiGa mostly produced hydrogen with some hydrocarbons and trace amounts of CO in 0.1 M Na_2CO_3 acidified to pH 6.8 with 1 atm CO_2 [20]. They found that the catalyst is more active towards ethane rather than ethylene. However, it is difficult to distinguish these two products using the DEMS setup at these production levels, since both products have a similar mass spectrum. Therefore, the activities towards both products could not be quantified in our system.

Finally, the results clearly show that, although most catalysts produce hydrocarbon products, all tested catalysts mostly produced hydrogen and were far from selective towards further CO_2RR products under the tested conditions. This observation is in contrast to the predictions made by screening papers that these materials would selectively produce C_{2+} or further reduced products. Possibly, due to the testing conditions in ambient, aqueous electrolytes, hydrogen evolution is quickly the dominant product due to the overwhelming presence of water and the low solubility of CO_2. Studies have shown that under elevated pressure where there is a higher amount of CO_2 present at the surface, the selectivity of different catalysts can shift significantly [24–26], for example, nickel and iron catalysts that produce mostly hydrogen at atmospheric pressures.

Alternatively, the surface composition or structure of the catalyst material during electrochemical testing could differ from the as-synthesised materials. Jovanov and coworkers found a similar discrepancy between prediction and experimental results on Au-Cd alloys [27]. They attributed this discrepancy to the dissolution of cadmium from the alloy. The $FeZn_4$ sample was observed to have some hydrogen formation at open circuit potential inferring some zinc dissolution. This could possibly explain why the $FeZn_4$ sample was not selective towards CO_2 reduction, while this was suggested by Li et al. [12]. Significant leaching of metals from the other alloys is very unlikely. If there would have been substantial leaching, there would have been an accompanying reduction reaction to the oxidation of the alloy components. However, no reduction products at open circuit potential for any of the other catalysts or a substantial unbalance in our faradaic efficiency balance during catalyst testing was observed. Alternatively, the in-situ surface crystal structure could be reformed due to the electrolyte or the applied potential as was observed on a PdAu electrode [28]. Further in-operando spectroscopy of the alloys could indicate whether this the case. Finally, the catalyst surfaces are unavoidably slightly oxidised either ex-situ or in-situ prior to the measurements. These oxides are reduced before or during the catalytic measurements. However, the reduction of these oxides can have an effect on the structure and surface roughness of the alloys during the measurements.

Nevertheless, our results stress the impact that the hydrogen evolution reaction has on the selectivity towards CO_2 reduction for a catalyst material. The effect of hydrogen affinity on a catalyst's CO_2RR selectivity was already highlighted by multiple researchers [29–31]. However, in computational CO_2RR screening studies, the hydrogen evolution reaction is often not considered. Therefore, we advocate for a more

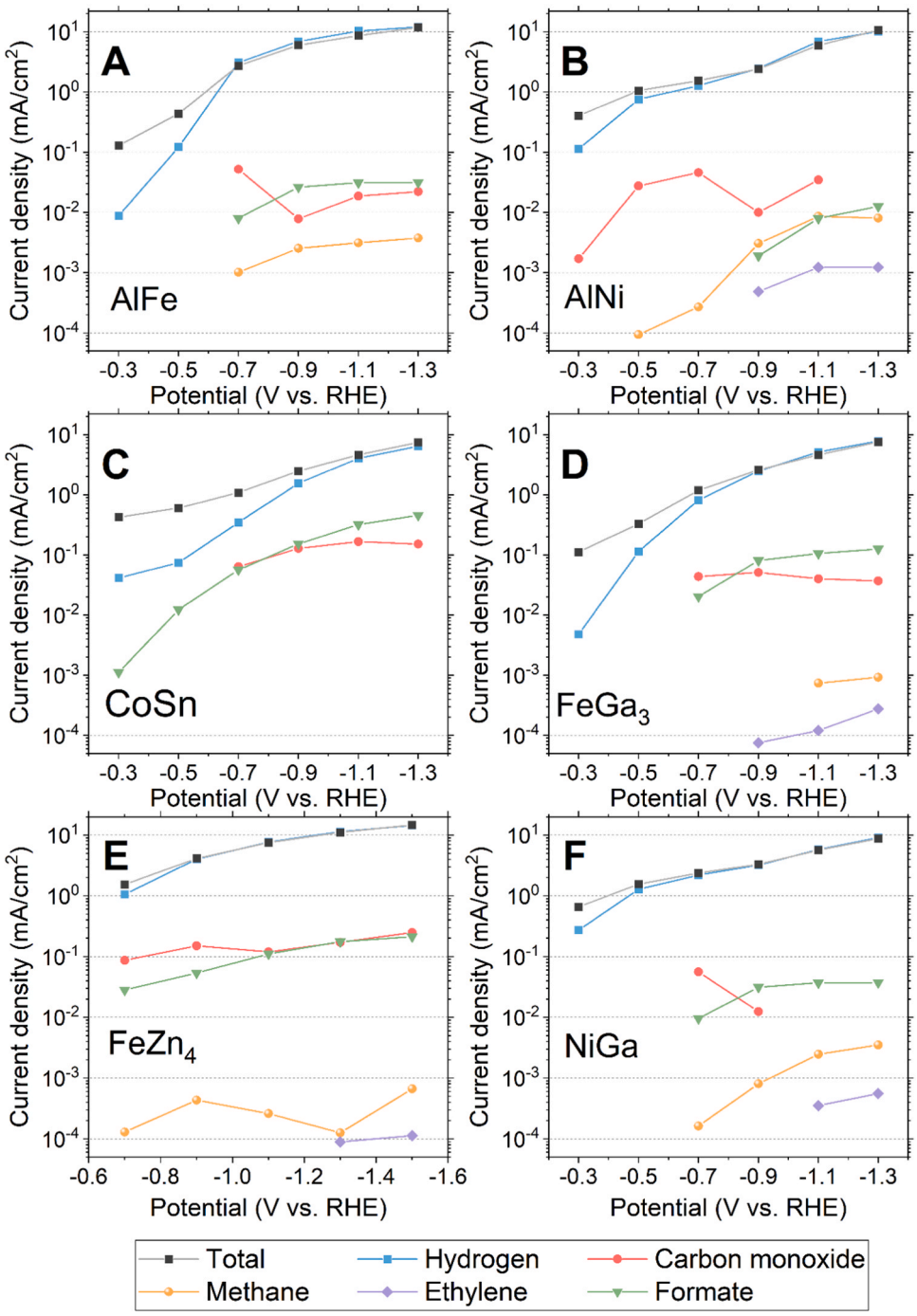

Fig. 2. Partial current densities for CO_2 reduction in a 0.1 M $KHCO_3$ buffer for AlFe, AlNi, CoSn, $FeGa_3$, $FeZn_4$, and NiGa. The major products observed on the electrodes are hydrogen (■), carbon monoxide (●), formate (▼), methane (●), and ethylene (◆). To indicate the activity of the catalyst and the complete quantification of all products, the total measured current density is shown as well (■).

holistic approach to CO_2RR catalyst screening where both the CO_2RR and the HER are taken into account. This practice is already more common for electrochemical nitrogen reduction screening papers [32, 33]. Furthermore, computational screening studies should also take into account a material's selectivity towards formate or CO. Many studies focus on the binding strengths of CO_2RR intermediates after the reduction to CO to screen catalyst materials towards further reduced products. However, this step could be premature as CO_2 first has to reduce to CO. Therefore, if this step is not favourable, formic acid is produced instead. However, finding a single descriptor to determine whether a catalyst is selective towards CO or formate has been proven difficult; no clear reason has been found why monometallic catalysts such as silver or gold are selective towards CO under experimental conditions but should be selective towards formate according to DFT simulations. Morrison and coworkers have shown that the surface coverage plays an important role in predicting whether a surface is selective towards CO or formate [34] while Christensen and coworkers show that the materials lattice constant could be used to classify materials [35]. Finding such a descriptor for alloys can greatly enhance the accuracy of computational screening methods.

Finally, screening papers often limit themselves to specific crystal structures or bimetallic compositions (A_3B or AB), due to the large

computational efforts that are involved in DFT calculations. However, these structures or compositions might not exist in reality or separate into two stable phase compositions. Examples of this can be found in literature where a catalyst material was synthesised with a specific initial composition, but in-situ segregated into two phases [36,37]. Also, several predicted alloys from Li et al. could not be synthesised in this study due to this reason (FeGa, FeZn). Therefore, instead of specific bimetallic compositions for all alloys, researchers should use databases of electronic structures of stable compositions to obtain usable predictions from computational screenings. For instance, Tran and co-workers already obtained their intermetallic combinations from the Materials project [38]. Alternatively, researchers could use phase diagrams to check if an alloy is (likely) to be stable at room temperature [39]. Without the use of these databases, computational time and effort are wasted on materials that are impossible to synthesise in practice.

4. Conclusion

We have synthesized and tested several intermetallic alloys for their CO_2 reduction reaction activity. Moreover, we have outlined a general method to produce these materials and several lessons that were learned. The alloy compositions were selected based on predictions highlighting their CO_2R selectivity towards further reduced products from previous computational screening papers. The selected compositions were AlFe, AlNi, CoSn, $FeGa_3$, $FeZn_4$, and NiGa. Almost all catalysts were shown to produce hydrocarbons (methane and ethylene), while CoSn was active towards formate production. Most materials that were characterised in this paper have not been tested before in the literature. Nevertheless, their results matched well with similar tested alloy materials in the literature. However, the materials were mostly active towards hydrogen formation and only had limited CO_2 reduction activity. We have postulated several reasons for this discrepancy and outlined several ways to improve CO_2RR screening methods. These results highlight the importance of experimental validation of DFT results and how modelling and experimental work should work together to iteratively find selective CO_2 reduction materials.

CRediT authorship contribution statement

Ruud Kortlever: Writing – review & editing, Supervision, Project administration, Funding acquisition, Conceptualization. **Ruud W.A. Hendrikx:** Writing – review & editing, Resources, Investigation. **Johannes C. Brouwer:** Writing – review & editing, Resources, Investigation. **Daniël van den Berg:** Writing – review & editing, Writing – original draft, Methodology, Investigation, Formal analysis, Conceptualization.

Declaration of Competing Interest

The authors declare that they have no known competing financial interests or personal relationships that could have appeared to influence the work reported in this paper.

Data availability

Data will be made available on request.

Appendix A. Supporting information

Supplementary data associated with this article can be found in the online version at doi:10.1016/j.cattod.2024.114805.

References

[1] Y. Hori, K. Kikuchi, S. Suzuki, Production of CO and CH_4 in electrochemical reduction of CO_2 at metal electrodes in aqueous hydrogencarbonate solution. Chem. Lett. 14 (11) (1985) 1695–1698, https://doi.org/10.1246/cl.1985.1695.

[2] S. Nitopi, E. Bertheussen, S.B. Scott, X. Liu, A.K. Engstfeld, S. Horch, B. Seger, I.E. L. Stephens, K. Chan, C. Hahn, J.K. Nørskov, T.F. Jaramillo, I. Chorkendorff, Progress and perspectives of electrochemical CO_2 reduction on copper in aqueous electrolyte. Chem. Rev. 119 (12) (2019) 7610–7672, https://doi.org/10.1021/acs.chemrev.8b00705.

[3] K.P. Kuhl, E.R. Cave, D.N. Abram, T.F. Jaramillo, New insights into the electrochemical reduction of carbon dioxide on metallic copper surfaces, Energy Environ. Sci. 5 (5) (2012) 7050–7059, https://doi.org/10.1039/C2EE21234J.

[4] S. Asperti, R. Hendrikx, Y. Gonzalez-Garcia, R. Kortlever, Benchmarking the electrochemical CO_2 reduction on polycrystalline copper foils: the importance of microstructure versus applied potential. ChemCatChem (2022) e202200540 https://doi.org/10.1002/cctc.202200540.

[5] A. Bagger, W. Ju, A.S. Varela, P. Strasser, J. Rossmeisl, Electrochemical CO_2 reduction: a classification problem. ChemPhysChem 18 (22) (2017) 3266–3273, https://doi.org/10.1002/cphc.201700736.

[6] M. Azuma, K. Hashimoto, M. Hiramoto, M. Watanabe, T. Sakata, Electrochemical reduction of carbon dioxide on various metal electrodes in low-temperature aqueous $KHCO_3$ media. J. Electrochem. Soc. 137 (6) (1990) 1772–1778, https://doi.org/10.1149/1.2086796.

[7] M. Azuma, K. Hashimoto, M. Watanabe, T. Sakata, Electrochemical reduction of carbon dioxide to higher hydrocarbons in a $KHCO_3$ aqueous solution. J. Electroanal. Chem. Interfacial Electrochem. 294 (1-2) (1990) 299–303, https://doi.org/10.1016/0022-0728(90)87154-C.

[8] H. Peng, M.T. Tang, X. Liu, P.S. Lamoureux, M. Bajdich, F. Abild-Pedersen, The role of atomic carbon in directing electrochemical CO_2 reduction to multicarbon products. Energy Environ. Sci. 14 (1) (2021) 473–482, https://doi.org/10.1039/D0EE02826F.

[9] F. Calle-Vallejo, J. Martínez, J.M. García-Lastra, J. Rossmeisl, M. Koper, Physical and chemical nature of the scaling relations between adsorption energies of atoms on metal surfaces, Phys. Rev. Lett. 108 (11) (2012) 116103, https://doi.org/10.1103/PhysRevLett.108.116103.

[10] S. Popović, M. Smiljanić, P. Jovanovič, J. Vavra, R. Buonsanti, N. Hodnik, Stability and degradation mechanisms of copper-based catalysts for electrochemical CO_2 reduction. Angew. Chem. 132 (35) (2020) 14844–14854, https://doi.org/10.1002/anie.202000617.

[11] J. Vavra, G.P. Ramona, F. Dattila, A. Kormányos, T. Priamushko, P.P. Albertini, A. Loiudice, S. Cherevko, N. Lopéz, R. Buonsanti, Solution-based Cu^+ transient species mediate the reconstruction of copper electrocatalysts for CO_2 reduction. Nat. Catal. 9 (1) (2024) https://doi.org/10.1038/s41929-023-01070-8.

[12] J. Li, J.H. Stenlid, M.T. Tang, H.-J. Peng, F. Abild-Pedersen, Screening binary alloys for electrochemical CO_2 reduction towards multi-carbon products. J. Mater. Chem. A 10 (30) (2022) 16171–16181, https://doi.org/10.1039/D2TA02749F.

[13] K. Tran, Z.W. Ulissi, Active learning across intermetallics to guide discovery of electrocatalysts for CO_2 reduction and H_2 evolution. Nat. Catal. 1 (9) (2018) 696–703, https://doi.org/10.1038/s41929-018-0142-1.

[14] X. Ma, Z. Li, L.E.K. Achenie, H. Xin, Machine-learning-augmented chemisorption model for CO_2 electroreduction catalyst screening. J. Phys. Chem. Lett. 6 (18) (2015) 3528–3533, https://doi.org/10.1021/acs.jpclett.5b01660.

[15] H. Hansen, C. Shi, A. Lausche, A. Peterson, J. Nørskov, Bifunctional alloys for the electroreduction of CO_2 and CO. Phys. Chem. Chem. Phys. 18 (13) (2016) 9194–9201, https://doi.org/10.1039/C5CP07717F.

[16] M.-J. Cheng, E.L. Clark, H.H. Pham, A.T. Bell, M. Head-Gordon, Quantum mechanical screening of single-atom bimetallic alloys for the selective reduction of CO_2 to C_1 hydrocarbons. ACS Catal. 6 (11) (2016) 7769–7777, https://doi.org/10.1021/acscatal.6b01393.

[17] A. Dasgupta, R.M. Rioux, Intermetallics in catalysis: an exciting subset of multimetallic catalysts, Catal. Today 330 (2019) 2–15, https://doi.org/10.1016/j.cattod.2018.05.048.

[18] A.R. Paris, A.B. Bocarsly, Mechanistic insights into C_2 and C_3 product generation using Ni_3Al and Ni_3Ga electrocatalysts for CO_2 reduction. Faraday Discuss. 215 (2019) 192–204, https://doi.org/10.1039/C8FD00177D.

[19] A.R. Paris, A.B. Bocarsly, Ni–Al films on glassy carbon electrodes generate an array of oxygenated organics from CO_2, ACS Catal. 7 (10) (2017) 6815–6820, https://doi.org/10.1021/acscatal.7b02146.

[20] D.A. Torelli, S.A. Francis, J.C. Crompton, A. Javier, J.R. Thompson, B. S. Brunschwig, M.P. Soriaga, N.S. Lewis, Nickel–gallium-catalyzed electrochemical reduction of CO_2 to highly reduced products at low overpotentials. ACS Catal. 6 (3) (2016) 2100–2104, https://doi.org/10.1021/acscatal.5b02888.

[21] D. Van den Berg, H.P. Lopuhaä, R. Kortlever, Direct Quantification of Electrochemical CO_2 Reduction Products with an Improved DEMS Setup, Submitted for Publication.

[22] O.K. von Goldbeck, Fe—Zn Iron—Zinc, IRON—Bin. Phase Diagr. (1982) 172–175, https://doi.org/10.1007/978-3-662-08024-5_79.

[23] A. Zhang, B. Mu, H. Li, X. An, A. Wang, Cobalt blue hybrid pigment doped with magnesium derived from sepiolite, Appl. Clay Sci. 157 (2018) 111–120, https://doi.org/10.1016/j.clay.2018.02.032.

[24] K. Hara, A. Kudo, T. Sakata, Electrochemical reduction of carbon dioxide under high pressure on various electrodes in an aqueous electrolyte, J. Electroanal. Chem. 391 (1-2) (1995) 141–147, https://doi.org/10.1016/0022-0728(95)03935-A.

[25] K. Hara, A. Kudo, T. Sakata, Electrochemical reduction of high pressure carbon dioxide on Fe electrodes at large current density, J. Electroanal. Chem. 386 (1-2) (1995) 257–260, https://doi.org/10.1016/0022-0728(95)03917-6.
[26] A. Kudo, S. Nakagawa, A. Tsuneto, T. Sakata, Electrochemical reduction of high pressure CO_2 on Ni electrodes. J. Electrochem. Soc. 140 (6) (1993) 1541–1545, https://doi.org/10.1149/1.2221599.
[27] Z.P. Jovanov, H.A. Hansen, A.S. Varela, P. Malacrida, A.A. Peterson, J.K. Nørskov, I.E.L. Stephens, I. Chorkendorff, Opportunities and challenges in the electrocatalysis of CO_2 and CO reduction using bifunctional surfaces: a theoretical and experimental study of Au–Cd alloys. J. Catal. 343 (2016) 215–231, https://doi.org/10.1016/j.jcat.2016.04.008.
[28] J.S. Jirkovský, I. Panas, S. Romani, E. Ahlberg, D.J. Schiffrin, Potential-dependent structural memory effects in Au–Pd nanoalloys, J. Phys. Chem. Lett. 3 (3) (2012) 315–321, https://doi.org/10.1021/jz201660t.
[29] R. Chaplin, A. Wragg, Effects of process conditions and electrode material on reaction pathways for carbon dioxide electroreduction with particular reference to formate formation, J. Appl. Electrochem. 33 (12) (2003) 1107–1123, https://doi.org/10.1023/B%3AJACH.0000004018.57792.B8.
[30] M. Jitaru, D. Lowy, M. Toma, B. Toma, L. Oniciu, Electrochemical reduction of carbon dioxide on flat metallic cathodes, J. Appl. Electrochem. 27 (1997) 875–889, https://doi.org/10.1023/A:1018441316386.
[31] A. Bagger, Reduction Reactions versus Hydrogen, Curr. Opin. Electrochem. 40 (2023) 101339, https://doi.org/10.1016/j.coelec.2023.101339.
[32] A. Bagger, H. Wan, I.E. Stephens, J. Rossmeisl, Role of catalyst in controlling N_2 reduction selectivity: a unified view of nitrogenase and solid electrodes. ACS Catal. 11 (11) (2021) 6596–6601, https://doi.org/10.1021/acscatal.1c01128.
[33] E. Skulason, T. Bligaard, S. Gudmundsdóttir, F. Studt, J. Rossmeisl, F. Abild-Pedersen, T. Vegge, H. Jónsson, J.K. Nørskov, A theoretical evaluation of possible transition metal electro-catalysts for N_2 reduction. Phys. Chem. Chem. Phys. 14 (3) (2012) 1235–1245, https://doi.org/10.1039/C1CP22271F.
[34] A.R. Morrison, V. van Beusekom, M. Ramdin, L.J. van den Broeke, T.J. Vlugt, W. de Jong, Modeling the electrochemical conversion of carbon dioxide to formic acid or formate at elevated pressures, J. Electrochem. Soc. 166 (4) (2019) E77, https://doi.org/10.1149/2.0121904jes.
[35] O. Christensen, A. Bagger, J. Rossmeisl, The missing link for electrochemical CO_2 reduction: classification of CO vs HCOOH selectivity via PCA, reaction pathways, and coverage analysis. ACS Catal. 14 (2023) 2151–2161, https://doi.org/10.1021/acscatal.3c04851.
[36] E.L. Clark, C. Hahn, T.F. Jaramillo, A.T. Bell, Electrochemical CO_2 reduction over compressively strained CuAg surface alloys with enhanced multi-carbon oxygenate selectivity. J. Am. Chem. Soc. 139 (44) (2017) 15848–15857, https://doi.org/10.1021/jacs.7b08607.
[37] S. Chandrashekar, N.T. Nesbitt, W.A. Smith, Electrochemical CO_2 reduction over bimetallic Au–Sn thin films: comparing activity and selectivity against morphological, compositional, and electronic differences. J. Phys. Chem. C 124 (27) (2020) 14573–14580, https://doi.org/10.1021/acs.jpcc.0c01894.
[38] A. Jain, S.P. Ong, G. Hautier, W. Chen, W.D. Richards, S. Dacek, S. Cholia, D. Gunter, D. Skinner, G. Ceder, Commentary: the materials project: a materials genome approach to accelerating materials innovation, APL Mater. 1 (1) (2013) 1–11, https://doi.org/10.1063/1.4812323.
[39] H. Okamoto, Desk Handbook: Phase Diagrams for Binary Alloys, first ed., ASM International, Materials Park, 2000.